International Journal of Fluid Machinery and Systems
Vol. 6, No. 1, January-March 2013

DOI: http://dx.doi.org/10.5293/IJFMS.2013.6.1.025
ISSN (Online): 1882-9554

Original Paper (Invited)

Internal Flow Condition of High Power Contra-Rotating Small-Sized Axial Fan

Toru Shigemitsu[1], Junichiro Fukutomi[1] and Takuya Agawa[2]

[1]Institute of Technology and Science, The University of Tokushima
2-1 Minamijosanjima-cho, Tokushima, 770-8506, Japan, t-shige@tokushima-u.ac.jp
[2]Graduate School of Advanced Technology and Science, The University of Tokushima
2-1 Minamijosanjima-cho, Tokushima, 770-8506, Japan

Abstract

Data centers have been built with spread of cloud computing. Further, electric power consumption of it is growing rapidly. High power cooling small-sized fans; high pressure and large flow rate small-sized fan, are used for servers in the data centers and there is a strong demand to increase power of it because of increase of quantity of heat from the servers. Contra-rotating rotors have been adopted for some of high power cooling fans to meet the demand for high power. There is a limitation of space for servers and geometrical restriction for cooling fans because spokes to support fan motors, electrical power cables and so on should be installed in the cooling fans. It is important to clarify complicated internal flow condition and influence of a geometric shape of the cooling fans on performance to achieve high performance of the cooling fans. In the present paper, the performance and the flow condition of the high power contra-rotating small-sized axial fan with a 40mm square casing are shown by experimental and numerical results. Furthermore, influence of the geometrical shape of the small-sized cooling fan on the internal flow condition is clarified and design guideline to improve the performance is discussed.

Keywords: Axial flow fan, Cooling fan, Performance, Internal flow

1. Introduction

Data centers have been built because of spread of cloud computing, establishment of ubiquitous networking society and increase in rate of electric parts in machines. Then, electric power consumption in the data centers, IT devices and machines have been increasing significantly[1]. Electric power used for cooling of the IT devices for the data centers is huge the same as that used for the IT devices itself in the data centers and the electric power consumption of it is growing rapidly. There is a strong demand for a reduction of electric power consumption in above facilities and equipments from the point of view of the global warming and the energy savings[2]. High power cooling small-sized fans; high pressure and large flow rate small-sized fan, are used for servers in the data centers and there is a strong demand to increase power of it because of increase of quantity of heat from the servers, however, increase of the power by an increase of a fan diameter is restricted because of limitation of space. Therefore, high rotational speed design is conducted, and the rotational speed over 10,000min^{-1} is employed for the cooling fans of servers. Contra-rotating rotors have been adopted for some of the high power cooling fans to meet the demand for high power. On the other hand, low rotational speed design[3] and advantages on the performance of the contra-rotating fans and pumps were verified by experimental results[4],[5]. In the case of contra-rotating rotors, an axial space becomes larger than conventional small-sized axial fans, but it is adequate choice to apply the contra-rotating rotors for small sized-fans because the axial space can be ensured in electrical devices as compared to that of a radial space. Influence of the axial space of the contra-rotating axial flow fan was investigated in a middle size fan[6] and a small-sized fan[7]. In the case of the contra-rotating rotors, it is necessary to design the rotor considering unsteady flow condition[8]. Further, it is important to clarify influence of wakes from a front rotor to a rear rotor on performance and pressure interaction between the front and the rear rotors[9]. Further, the conventional design method and the theory for turbo machinery should be modified for small-sized axial fans because small-sized axial fans applied to electrical devices belong to extremely small size field in turbo machinery[10]. In addition to that, there is a limitation of space for servers and geometrical restriction for cooling fans because spokes to support the fan motor, electrical power cables and so on should be installed in the cooling fans. Therefore, it is important to clarify complicated internal flow condition and influence of the

Received June 22 2012; revised January 12 2013; accepted for publication February 28 2013: Review conducted by Prof. Hyung-Hee Cho. (Paper number O13002S)
Corresponding author: Toru Shigemitsu, Associate Professor, t-shige@tokushima-u.ac.jp

This paper was presented at 5th International Symposium on Fluid Machinery and Fluids Engineering, October 24-27, 2012, Jeju, Korea.

geometric shape of the cooling fans on performance to achieve the high performance cooling fans. It is thought especially for the case of the high power small-sized cooling fans that the internal flow condition is complicated because of complex geometry and design specification of high pressure and large flow rate. Then, the internal flow condition of the high power cooling fans is not clarified. Furthermore, the performance in detail of each front and rear rotor is not known because of extreme compact size of the high power contra-rotating small-sized cooling fans. In the present paper, pressure curves of a contra-rotating small-sized axial fan with a 40mm square casing are shown by the experimental and the numerical results. Difference of the pressure curves of each front and rear rotor is discussed. Furthermore, influences of the geometrical shape and the design specification of the high power small-sized cooling fan on internal flow condition are clarified and design guideline to improve the performance is considered.

2. Experimental Procedure and Numerical Analysis Conditions

2.1 Experimental Apparatus and Method

The test fan and the primary dimensions of the high power contra-rotating small-sized axial fan(R40W-A) are shown in Fig.1 and Table 1 respectively. The rotors of R40W-A was set in the 40mm square casing, and a hub tip ratio of the front and the rear rotors were D_{hf}/D_{tf}=25mm/37.2mm=0.67 and D_{hr}/D_{tr}=26mm/37.2mm=0.70 respectively. An operating flow rate was Q_o=0.55m^3/min and a tip clearance c=0.6mm. Design rotational speed of the front and the rear rotors of R40W-A were extremely high as N_f= 15000min^{-1} and N_r=14000min^{-1}. Figure 2 shows a schematic diagram of an experimental apparatus. The experimental apparatus was designed based on the Japanese Industrial Standard and air blown in a test section passed the rotors, a chamber, a measurement duct and a booster fan and blew out in the ambient atmosphere. Each rotor was driven by a brushless motor set inside of the hub and the motor was supported by spokes connected to the casing. The rotational speed of each rotor was kept constant (N_f=15000min^{-1}, N_r=14000min^{-1}) by a PWM control using a function generator when a performance test was conducted. Fan static pressure (ΔP) was measured by pressure difference between static holes downstream of the rotor installed at the chamber and ambient air. Further, the rotational speed was evaluated using a pulse of the motor measured by an oscilloscope. The flow rates were measured by an orifice meter set at the measurement duct and the pressure curves from a cutoff flow rate to large flow rate were investigated in the experiment. There were three spokes downstream of the front and the rear rotors to support the motors and the casing had a corner curve at an inlet and an outlet of the casing and a roundness between the front and the rear rotor as could be confirmed by a sectional view of the R40W-A in Fig.3. Therefore, there were some geometrical restrictions for the high power cooling small-sized fan.

2.2 Numerical Analysis Method and Conditions

The commercial software ANSYS-CFX13 was used to investigate the flow condition which couldn't be measured by the experiment and three dimensional unsteady numerical analysis was conducted. Figure 4 shows a numerical model used for the numerical flow analysis. In the numerical model, in order to improve accuracy of the numerical results, a simplification of the numerical model was conducted by removing spokes downstream of each rotor, extension of the length of the front rotor hub to the rear rotor inlet and so on as could be found by comparing Fig.3 to Fig.4. Numerical grids used for the numerical analysis are shown in Fig.5. The numerical domains comprised the inlet, the rotor, the chamber and the outlet duct regions. The numerical grid points were 554,345 for the inlet region, 1,170,773 for the chamber region and the outlet duct region. The numerical grid points for the rotor region were 4,520,095 and 4,024,967 for the front and the rear rotors respectively. The tip clearance was kept 0.6mm as the same with the experimental apparatus in the numerical analysis. At the inlet boundary, the constant flow rate was given and the constant pressure was given as the outlet boundary condition. The coupling between the front and the rear rotors was accomplished by the transient rotor stator. Standard wall function and LRR Reynolds Stress model was used as a turbulence model. The unsteady numerical flow analysis was conducted at the operating flow rate Q_o=0.55m^3/min and 3 other flow rate points Q=0.6, 0.7, 0.8 m^3/min. Time step number per one rotor rotation was 140 and the time step was t=2.857×10^{-5} s. Data of one rotor rotation were obtained after 10 rotor rotations in the unsteady numerical analysis.

Fig. 1 Picture of R40W-A

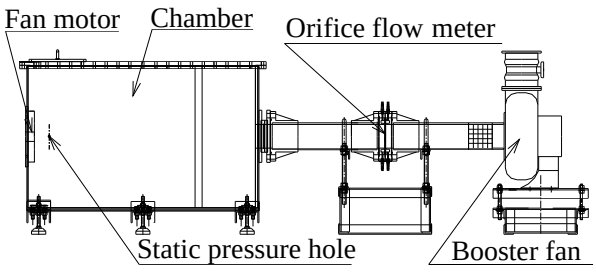

Fig. 2 Schematic diagram of experimental apparatus

Table 1 Primary dimensions of rotors

		Hub	Mid	Tip
Front Rotor	Diameter [mm]	25	31.1	37.2
	Blade Number	7		
	Solidity	1.61	1.4	1.22
	Stagger Angle [deg]	18.2	31.2	36
Rear Rotor	Diameter [mm]	26	3.16	37.2
	Blade Number	5		
	Solidity	1.03	1.17	1.1
	Stagger Angle [deg]	40.6	40	45.5

The fan static pressure for the numerical analysis was calculated by the static pressure difference between the static holes positions installed at the chamber and the inlet boundary of the numerical domain, which was almost the same with the experiment. On the other hand, the fan static pressure of the front rotor was evaluated by mass averaged static pressure difference of a sectional area at a middle axial position between the front and the rear rotor (z=24mm) and the inlet of the numerical domain. z is an axial position from the fan inlet. The rear rotor fan static pressure was also calculated by static pressure difference of a sectional area between the static holes position of the chamber (z=136mm) and the middle axial position between the front and the rear rotors. Further, dynamic and total pressure of each front and rear rotor were calculated by the same way at the same positions of the fan static pressure evaluation. Mass averaged data were obtained by the following Mass flow average abs function defined by the CFX.

$$\Phi = \frac{\Sigma(|m|\Phi)}{\Sigma|m|} \qquad (1)$$

where Φ represents a variable being averaged and m represents local mass flow. The air was assumed incompressive fluid, so the density of the air was constant in this research.

1. Experimental and Numerical Results

The pressure curves of R40W-A obtained by the experiment and the numerical analysis at the design rotational speed (N_f=15000min^{-1}, N_r=14000min^{-1}) are shown in Fig.6. A horizontal axis is flow rate Q and a vertical axis is fan static pressure ΔPs. The maximum fan static pressure was obtained at Q_o=0.55m^3/min by the experiment, however the maximum fan static pressure was obtained at Q=0.6m^3/min by the numerical analysis. Further, the maximum difference of the fan static pressure between the experiment and the numerical analysis was 22% at Q=0.6m^3/min. The discrepancy between the experiment and the numerical analysis could be caused by the design specification of high power small-sized cooling fan; a compact size with 40mm square casing, high pressure and large flow rate and the complex geometry of the numerical model, although the simplification was conducted compared to the experimental test model. On the other hand, the difference of the flow rate between the experiment and the numerical analysis, where the maximum fan static pressure was obtained, were within 5% and a similarity of the negative slope of the fan static pressure was confirmed between the experiment and the numerical analysis. Therefore, it was considered that the numerical analysis could capture the qualitative tendency of the experimental results to some extent and the pressure curves of each front and rear rotor and internal flow conditions were investigated by the unsteady numerical analysis results. It was found from Fig.6 that the fan static pressure of the front rotor was lower than that of the rear rotor and the fan static pressure of both front and rear rotors decreased with the increase of the flow rate. The fan static pressure of the rear rotor was high that the rate of the rear rotor fan static pressure to the total fan static pressure was about 78% at the operating flow rate Q_o=0.55m^3/min and the rate increased according to the increase of the flow rate.

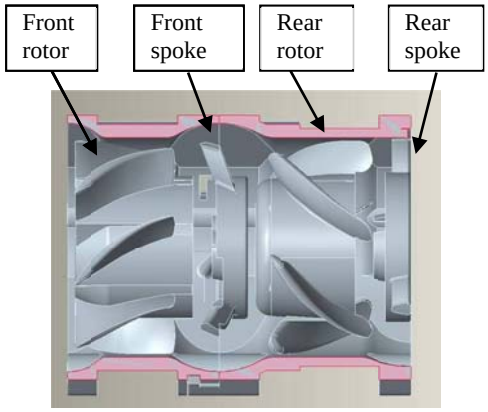

Fig. 3 Sectional view of casing for R40W-A

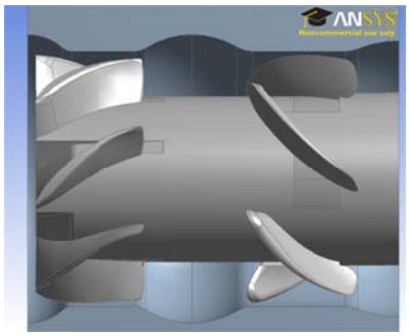

Fig. 4 Sectional view of calculation model

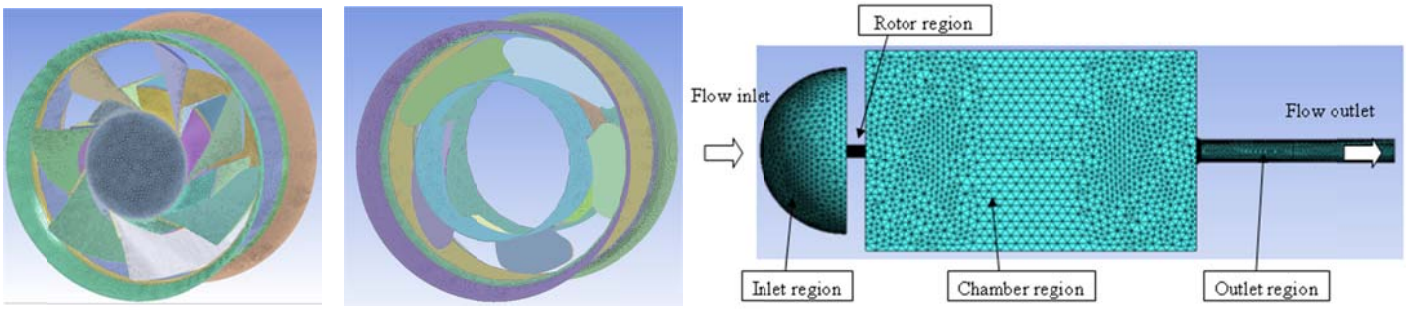

(a) Front rotor (b) Rear rotor (c) Whole regions

Fig. 5 Numerical grids

Dynamic and total pressure curves of the front and the rear rotors obtained by the numerical analysis are shown in Figs.7 and 8. The dynamic pressure of the front rotor was large and almost constant in all flow rates, where numerical analysis was conducted. On the contrary, the dynamic pressure of the rear rotor showed the negative value. These results in Figs.6 and 7 demonstrated that large dynamic pressure of the front rotor was recovered as the static pressure by the rear rotor. The total pressure showed the maximum value at Q=0.6m^3/min and that of the front rotor was higher than that of the rear rotor in Fig.8. These results indicated that the front rotor gave more dynamic pressure than the static pressure and high pressure gradient could work on the rear rotor because of the large increase of the static pressure with the conversion of the dynamic pressure from the front rotor to the static pressure by the rear rotor.

The internal flow conditions at the operating flow rate Q_o=0.55m^3/min with the rotor rotation were investigated by the numerical analysis results. Meridional velocity vectors on the vertical plane at the inlet of the front rotor with the operating flow rate Q_0=0.55m^3/min are shown in Fig.9. A rotational direction of the front rotor is front side of the paper and that of the rear rotor is back side of the paper. θ_f and θ_r represent rotation angles of each front and rear rotor leading edge from the meridional plane. θ_f=0deg and θ_r=0deg correspond a circumferential position that the leading edge of each front and rear rotor accords the meridional plane. The relative circumferential position of each front and rear rotor is the rear rotor rotation angle is θ_r=7.7deg when the front rotor rotation angle is θ_f=0.0deg. Focused on the flow condition in Fig.9(a) when leading edge of the front rotor accorded with the meridional plane(θ_f=0.0deg), a vortex occurred at the inlet corner curve and this vortex could be caused by the separation of the main flow around the inlet corner. The region of the vortex became large and the vortex existed from the corner curve to the blade tip when the front rotor passed the meridional plane about 20% of the chord length (θ_f=10.3deg) in Fig.9(b). Influence of the vortex on the main flow at the inlet of the front rotor was not so large by θ_f=10.3deg because the vortex remained at the corner curve at the inlet. On the other hand, the vortex moved downstream inside of the front rotor when the front rotor passed the meridional plane 50% of the chord length (θ_f=25.7deg) in Fig.9(c), and the flow condition near the tip of the front rotor was influenced by this vortex.

Blade-to-blade relative velocity of the front rotor at r/r_c=0.98 are shown in Fig.10. The flow rate was the operating flow rate Q_o. r and r_c means radius, where the data obtained, and radius of the casing. It was observed from Figs.10(a) and (b) that the leakage flow from a pressure surface to a suction surface near the mid of the blade chord were confirmed. The vortex observed in Fig.9(c) in the meridional plane related to the leakage flow from the blade tip. Further, the vortex observed in Fig.9(b) could be caused by the mixture of the corner separation and the leakage flow from the blade tip in Fig.10(b).

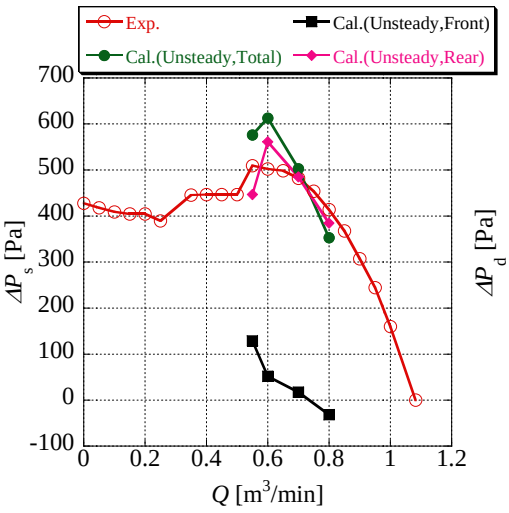

Fig. 6 Fan static pressure curves

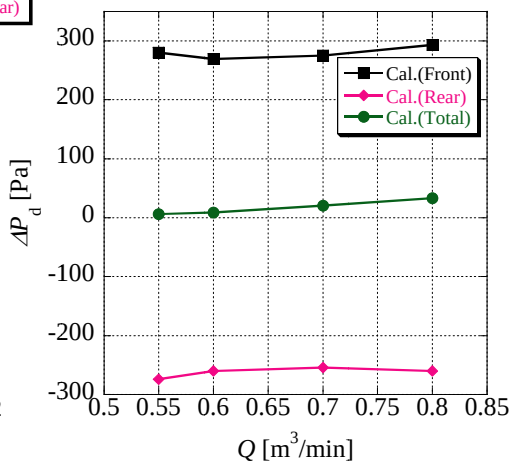

Fig. 7 Dynamic pressure curves

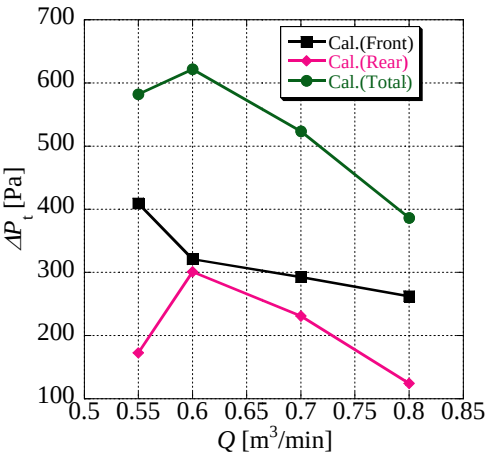

Fig. 8 Total pressure curves

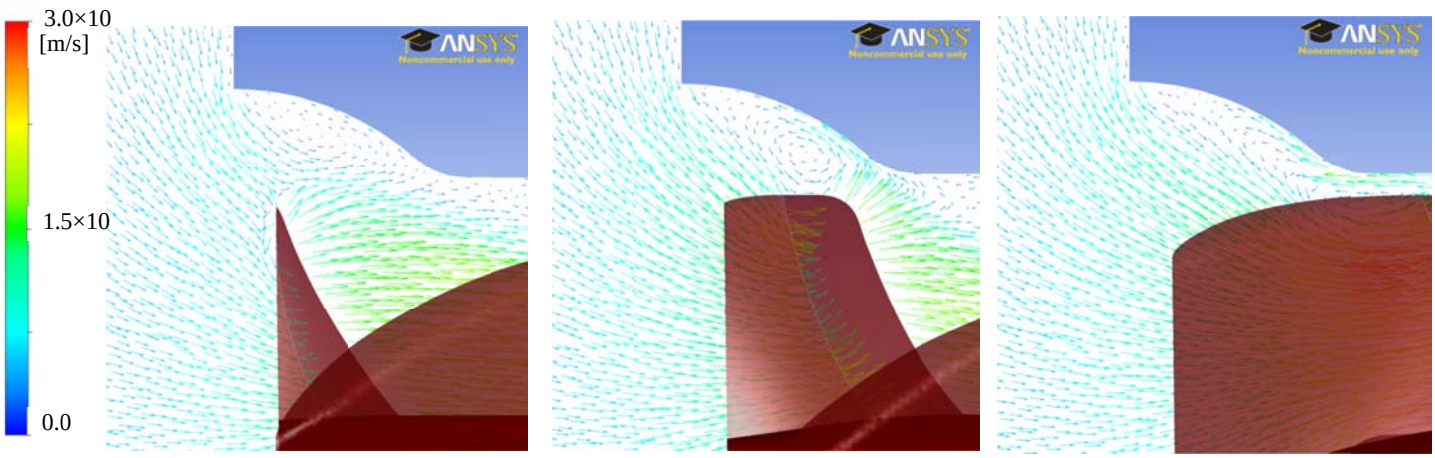

(a) θ_f=0.0[deg.] (b) θ_f=10.3[deg.] (c) θ_f=25.7[deg.]

Fig. 9 Meridional velocity vectors at inlet of front rotor

The meridional velocity vectors on the vertical plane of the front rotor at the operating flow rate Q_o=0.55m^3/min are shown in Fig.11. The rotational direction of the rotors, the rotation angles of each front and rear rotor and the relative circumferential position of each front and rear rotor were the same with those in Fig.9. Low axial velocity was observed in wide region on the meridional plane in Fig.11 and the low velocity region spread radially inner section when the front rotor passed the meridional plane about 30% of the chord length (θ_f=15.4deg) in Fig.11(a). This flow condition caused the inclined flow to the hub side in the front rotor. After that, the low velocity region shrunk and the strong vortex could be confirmed near the shroud in Fig.11(b) and the vortex near the shroud became small when the blade almost passed the meridional plane in Fig.11(c).

The meridional velocity vectors on the vertical plane between the front and the rear rotors at the operating flow rate Q_o=0.55m^3/min are shown in Fig.12. The rotational direction of the rotors, the rotation angles of each front and rear rotor and the relative circumferential position of each front and rear rotor were the same with those in Fig.9. The low velocity region became large between the front and the rear rotors when the front rotor passed the meridional plane about 65% of the chord length (θ_f=33.4deg) in Fig.12(a) and the low velocity region became small when the front rotor passed the meridional plane about 95% of the chord length (θ_f=48.9deg) in Fig.12(b). On the other hand, the flow condition at the inlet of the rear rotor became uniform in Figs.12(a) and (b), however the flow condition at the outlet of the front rotor was not uniform in the case θ_f=33.4deg in Fig.12(a).

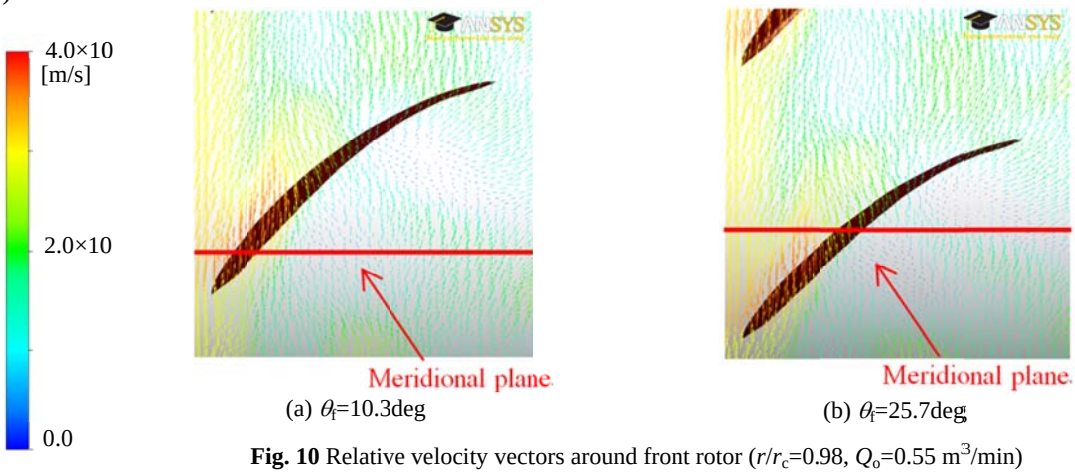

(a) θ_f=10.3deg (b) θ_f=25.7deg

Fig. 10 Relative velocity vectors around front rotor (r/r_c=0.98, Q_o=0.55 m^3/min)

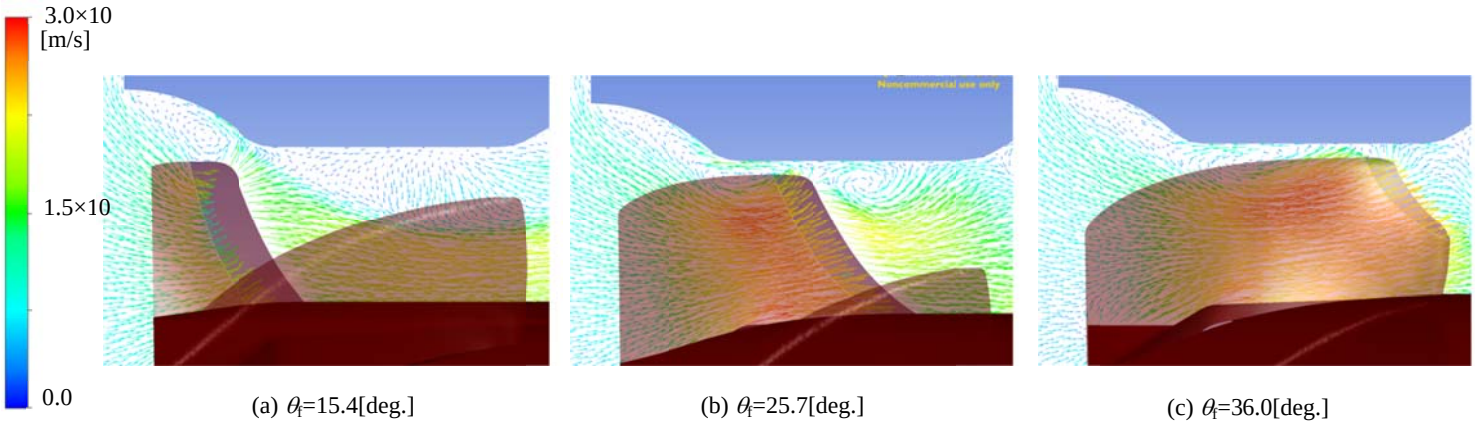

(a) θ_f=15.4[deg.] (b) θ_f=25.7[deg.] (c) θ_f=36.0[deg.]

Fig. 11 Meridional velocity vectors of front rotor

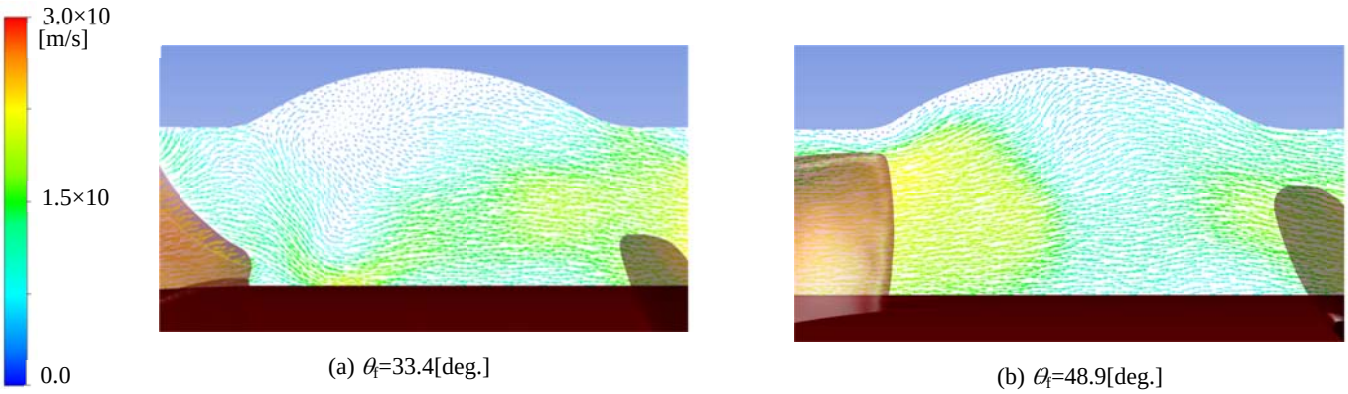

(a) θ_f=33.4[deg.] (b) θ_f=48.9[deg.]

Fig. 12 Meridional velocity vectors between front and rear rotors

Figures 13(a) and (b) show axial velocity and circumferential velocity obtained by the numerical analysis at the operating flow rate Q_o=0.55m^3/min in radial direction at the outlet of the front rotor and the inlet of the rear rotor respectively. The vertical axis is non-dimensional radius divided by the radius at the casing; r/r_c=0.65 and r/r_c=1.0 correspond the hub and the shroud. The circumferential velocity V_t is a positive in the direction of the front rotor rotation and the axial and the circumferential velocity were the average data of each rotation angle in one rotor rotation. The axial positions of the outlet of the front rotor and the inlet of the rear rotor, where the data were obtained, were 1mm downstream of the front rotor trailing edge and 1mm upstream of the rear rotor leading edge respectively. The axial velocity at the outlet of the front rotor was low near the shroud and became high near the hub region by the decrease of the velocity near the shroud. On the other hand, the axial velocity at the inlet of the rear rotor became uniform. The axial distance between the front and the rear rotor was short and it was clarified by the previous research that the axial velocity distribution between the front and the rear rotors did not change drastically in the case of the contra-rotating small-sized axial fan[11]. Therefore, the axial velocity at the inlet of the rear rotor would become uniform due to the casing with the roundness between the front and the rear rotor. On the other hand, the circumferential velocity distributions were complex that there were two peaks of the circumferential velocity near the shroud and the hub at the outlet of the front rotor and the inlet of the rear rotor and the circumferential velocity decreased at the inlet of the rear rotor except the region near the hub.

The meridional velocity vectors on the vertical plane of the rear rotor at the operating flow rate Q_o=0.55m^3/min are shown in Fig.14. The rotational direction of the rotors, the rotation angles of each front and rear rotor and the relative circumferential position of each front and rear rotor were the same with those in Fig.9. It could be found that there were a back flow and a vortex near the shroud and the hub. Further, the size of the vortex became large with the rotor rotation and the axial velocity at the mid of the span increased by a blockage effect of the vortex near the shroud and the hub in Figs.14(a) and (b). The blade-to-blade relative velocity of the rear rotor at r/r_c=0.98 are shown in Fig.15. The flow rate was the operating flow rate Q_o. Leakage flow from the

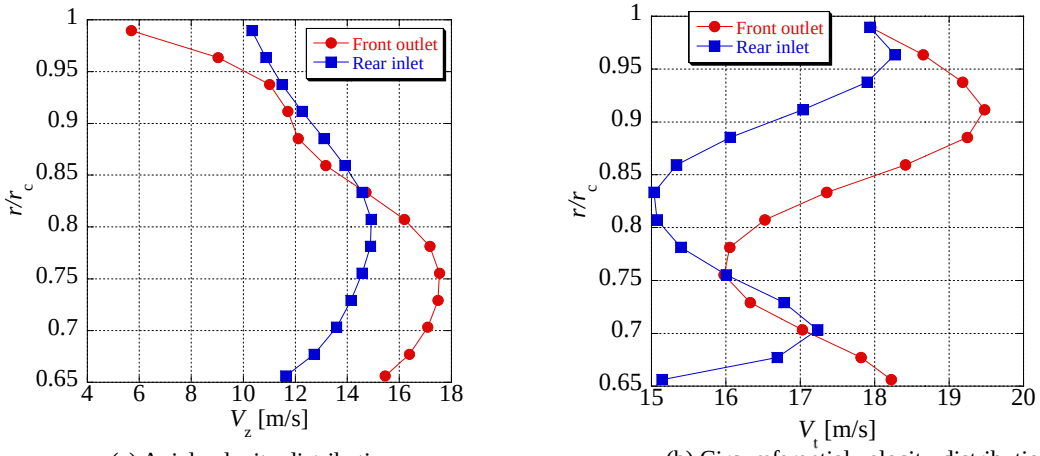

(a) Axial velocity distributions (b) Circumferential velocity distributions

Fig. 13 Velocity distributions at outlet of front rotor and inlet of rear rotor

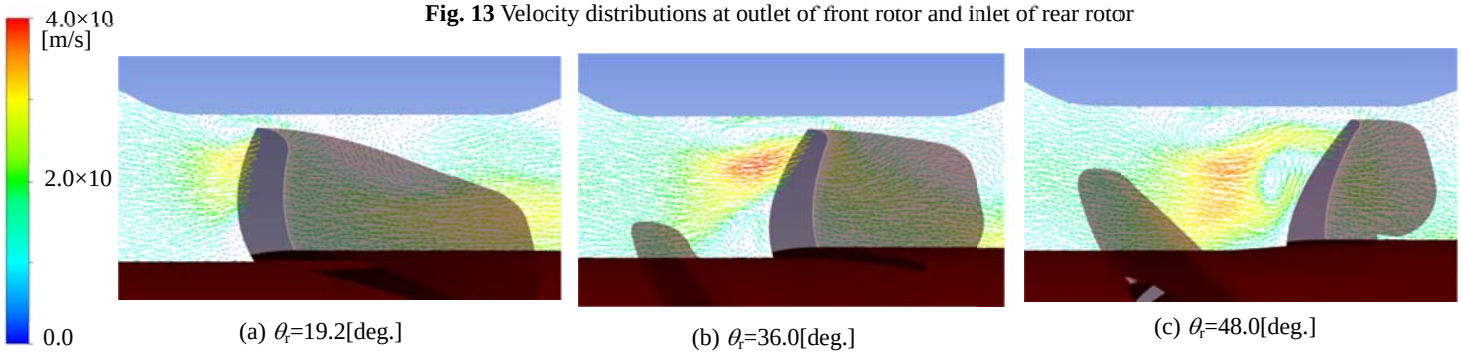

(a) θ_r=19.2[deg.] (b) θ_r=36.0[deg.] (c) θ_r=48.0[deg.]

Fig. 14 Meridional velocity vectors of rear rotor

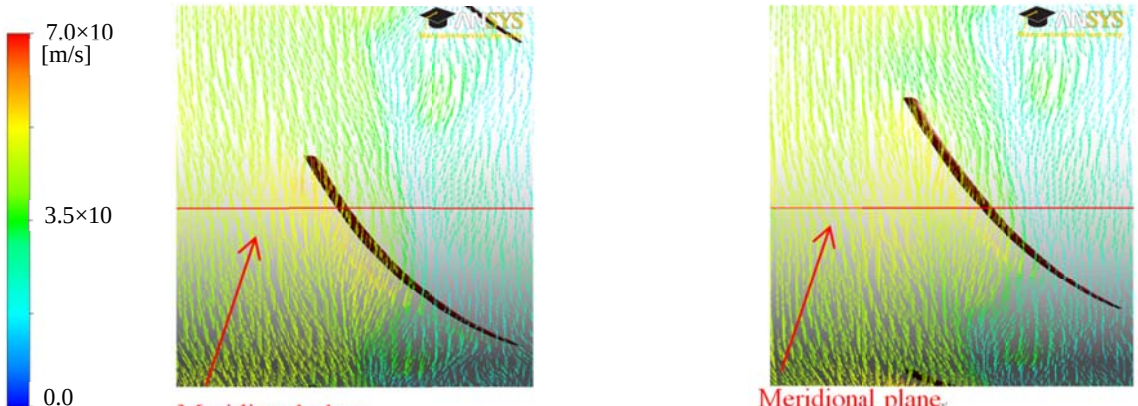

(a) θ_r=19.2 ° (b) θ_r=36.0 °

Fig. 15 Relative velocity vectors around rear rotor (r/r_c=0.98, Q_o=0.55 m^3/min)

pressure surface to the suction surface near the mid of the blade chord were confirmed in Figs.15(a) and (b). The back flow region related to the leakage flow of the rear rotor was larger than that of the front rotor. The blade-to-blade relative velocity of the rear rotor at r/r_c=0.81, which is the mid of the span, are shown in Fig.16. It could be found that a separation occurred on the suction surface near 60% of the blade chord. These would be caused by large adverse pressure gradient in the axial direction of the rear rotor that could be confirmed by the pressure curves in Fig.6. Therefore, the pressure gradient in the axial direction of each front and rear rotor should be modified for improvement of the performance; the fan static pressure balance between the front and the rear rotors should be modified. Figures 17(a) and (b) show the axial velocity and the circumferential velocity obtained by the numerical analysis at operating flow rate Q_o in radial direction at the outlet of the rear rotor respectively. The circumferential velocity V_t is a positive in the direction of the rear rotor rotation and the axial and the circumferential velocity were the average data of each rotation angle in one rotor rotation. The axial position of the outlet of the rear rotor was 1mm downstream of the rear rotor trailing edge. The axial velocity near the shroud was low and flow at the outlet of the rear rotor inclined to the hub side. The maximum axial velocity was over 20m at the outlet of the rear rotor. On the other hand, the relatively large circumferential velocity existed at the outlet of the rear rotor at the operating flow rate Q_o. The circumferential velocity downstream of the rear rotor could become the loss, so the reduction of the circumferential velocity downstream of the rear rotor is important to improve the performance.

4. Concluding Remarks

The pressure curves of high pressure and large flow rate small-sized contra-rotating axial flow fan were investigated by the experiment and the numerical analysis. In addition to that, the internal flow conditions at the operating flow rate were clarified by the numerical analysis results. As a result, following concluding remarks were obtained.

1. The fan static pressure of the rear rotor was larger than that of the front rotor. On the other hand, the total pressure of the front rotor was larger than that of the rear rotor.

2. There were the large back flow regions near the shroud of the casing in both front and rear rotors. The back flow region near the shroud of the rear rotor was larger than that of the front rotor. The balance of the fan static pressure between the front and the rear rotors should be modified for the further increase of the performance.

3. The circumferential velocity remained downstream of the rear rotor at the operating flow rate. Therefore, the deduction of the circumferential velocity is important to reduce the loss downstream of the fan.

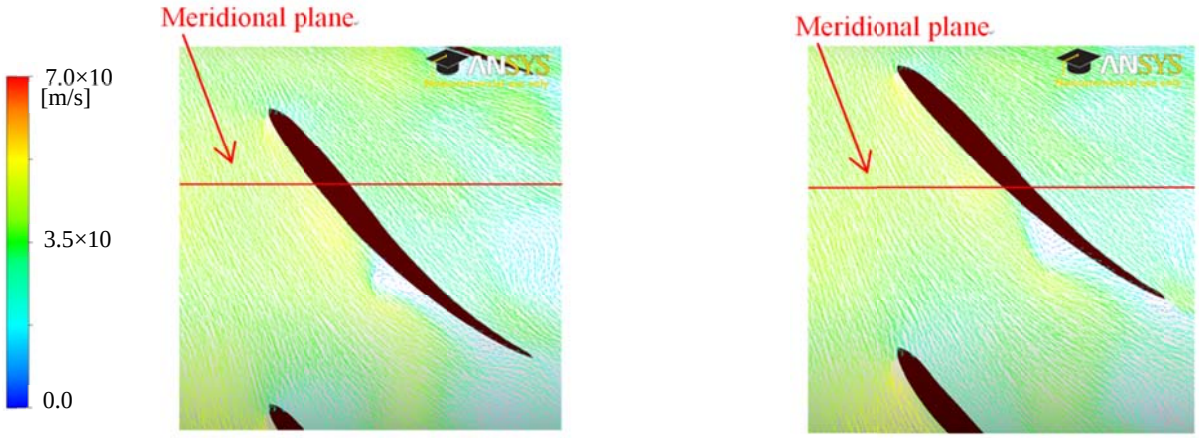

(a) θ_r=19.2 ° (b) θ_r=36.0 °

Fig. 16 Relative velocity vectors around rear rotor (r/r_c=0.81, Q_o=0.55 m^3/min)

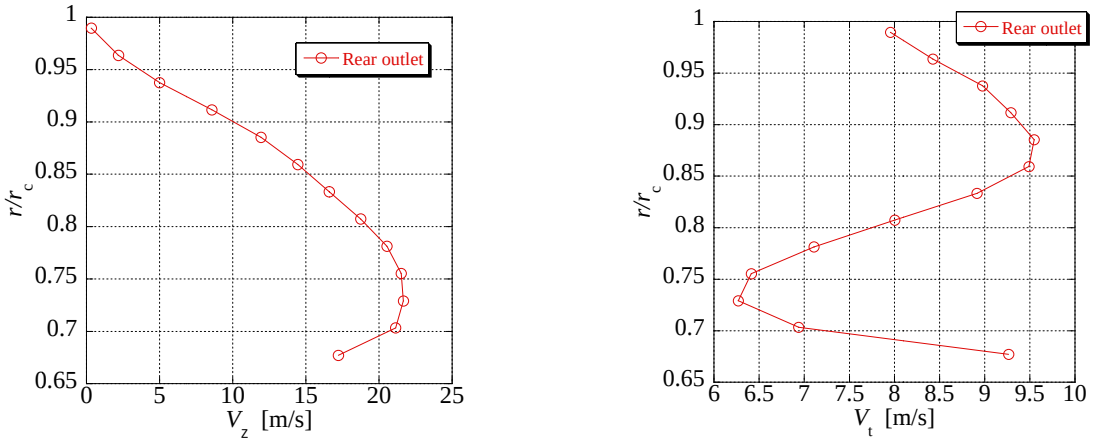

(a) Axial velocity distributions (b) Circumferential velocity distributions

Fig. 17 Velocity distributions at outlet of rear rotor

Acknowledgment

The authors wish to show our special thanks to the supports by Nidec Corporation, the project research aid from The University of Tokushima, Japan Science and Technology Agency and Komiya research aid.

Nomenclature

c	Tip clearance [mm]	Q_o	Operating flow rate [m^3/min]
D_h	Diameter of hub [mm]	r	Radius [mm]
D_t	Diameter of tip [mm]	r_c	Radius of casing [mm]
m	Local mass flow[kg/s]	z	Axial position from front rotor inlet[mm]
N	Rotational speed [min^{-1}]	Φ	Variable
N_d	Design rotational speed [min^{-1}]	θ	Rotational angle [°]
ΔP_d	Dynamic pressure [Pa]	**Subscripts**	
ΔP_s	Fan static pressure[Pa]	f	Front rotor
ΔP_t	Total pressure [Pa]	r	Rear rotor
Q	Flow rate [m^3/min]	d	Design point

References

[1] Hata, T. and Nakamoto, S., 2010, “Energy Saving Service for Data Centers,” J. the Japan Society for Precision Engineering, Vol. 76, No. 3, pp. 272-275.
[2] Miyahara, M. and Fukano, T., 2006, “Fan Cooling Technology for Small Electronic Device,” Turbomachinery(in Japanese), Vol. 34, No. 3, pp. 129-134.
[3] Furukawa, A., Shigemitsu, T. and Watanabe, S., 2007, “Performance Test and Flow Measurement of Contra-Rotating Axial Flow Pump,” J. Thermal Science, Vol. 16, No. 1, pp. 7-13.
[4] Furukawa, A., Cao, Y., Okuma, K. and Watanabe, S., 2000, “Experimental Study of Pump Characteristics of Contra-Rotating Axial Flow Pump,” Proc. 2nd Int. Symp. on Fluid Machinery and Fluid Eng., Beijing, 67-657, pp. 245-252.
[5] Kodama, Y., Hayashi, H., Fukano, T. and Tanaka, K., 1994, “Experimental Study on the Characteristics of Fluid Dynamics and noise of a Counter-Rotating Fan(1st Report, Effects of the Supporter Shape of the Electric Motor and the Distance between Two Rotors on the Characteristics) ,” Trans. JSME (in Japanese), Vol. 60, No. 576, pp. 2764-2771.
[6] Nouri, H., Ravelet, F., Bakir, F. and Sarraf, C., 2012, “Design and Experimental Validation of a Ducted Counter-Rotating Axial-Flow Fans System,” ASME J. Fluids Engineering, Vol. 134, No. 10, 104504.
[7] Shigemitsu, T., Fukutomi, J. and Shimizu H., 2012, “Influence of Blade Row Distance on Performance and Flow Condition of Contra-Rotating Small-Sized Axial Fan,” International Journal of Fluid Machinery and Systems, Vol. 5, No. 4, pp. 161-167.
[8] Shigemitsu, T., Furukawa, A., Okuma, K. and Watanabe, S., 2002, “Experimental Study on Rear Rotor Design in Contra-Rotating Axial Flow Pump,” Proc. 5th JSME/KSME Fluids Eng. Conf., Nagoya, pp. 1543-1548.
[9] Sanders, A., J., Papalia, J. and Fleeter, S., 2002, “Multi-Blade Row Interactions in a Transonic Axial Compressor: Part I- Stator Particle Image Velocimetry (PIV) Investigation,” ASME J. Turbomachinery, Vol. 124, No.1, pp. 10-18.
[10] Shigemitsu, T., Fukutomi, J. and Okabe, Y., 2010, “Performance and Flow Condition of Small-Sized Axial Fan and Adoption of Contra-Rotating Rotors,” J. Thermal Science, Vol. 19, No. 1, pp. 1-6.
[11] Shigemitsu, T., Fukutomi, J., Okabe, Y. and Iuchi, K., 2010, “Performance and Flow Condition of Contra-rotating Small-sized Axial Fan at Partial Flow Rate,” International Journal of Fluid Machinery and Systems, Vol. 3, No. 4, pp. 271-278.